Meyer, H. J. (1969) Struktur und Fehlordnung des Vaterits. *Z. Kristallogr.* **128**, 183 212.

Phemister, D. B., Aounsohn, M. G., and Pepensky, R. (1939) Variations in the cholesterol bile pigment and calcium salts contents of gallstones formed in gall-bladder and in bile ducts with the degree of associated obstruction. *Ann. Surg.* **109**, 161–86.

Rodgers, A. L. (1983) Common ultrastructural features in human calculi. *Micron Microscopia Acta*, **14**, 219–24.

Department of Mineralogy,   A. J. EASTON
Department of Central Services, British Museum (Natural History),   D. CLAUGHER
Cromwell Road, London SW7 5BD

Some observations on the chemical composition of todorokite

TODOROKITE is one of the major manganese oxide minerals in marine ferromanganese nodules occurring on the ocean floor, and it also occurs in significant amounts in terrestrial manganese deposits, in weathering zones and in soils. Discovered fifty years ago in Japan as a weathering product of inesite, $Ca_2Mn_7Si_{10}O_{28}(OH)_2 \cdot 5H_2O$ (Yoshimura, 1934), its structure and chemical composition are still matters of debate. Uncertainties as to structure arose chiefly because its X-ray powder diffraction pattern was somewhat similar to that of a sodium manganese manganate hydrate synthesized by Wadsley (1950) and because this pattern was also similar to one of the patterns observed in marine ferromanganese nodules by Buser and Grutter (1956). The phase producing this particular pattern was named by Buser (1959), 10 Å manganite. The controversy over the nature of these marine, terrestrial, and synthetic phases has produced an abundant literature (Burns and Burns, 1977, 1979) but little consensus of opinion. Agreement has however been reached over the status of todorokite (Giovanoli, 1985; Burns *et al.*, 1985).

During the last decade electron microscopy (EM), both scanning (SEM) and high resolution transmission (HRTEM), has been increasingly used in the study of these phases. At optical magnifications, terrestrial todorokite appears as prismatic crystals or as masses of parallel fibres (Chukhrov *et al.*, 1978, 1980). Under the SEM marine todorokite has been identified as fibrous masses (Burns and

Burns, 1978) and as platelets (Lallier-Verges and Clinard, 1983). The use of HRTEM has given abundant evidence that the plate morphology is really the result of sheets of fibres (Giovanoli, 1980) which at high magnification show dark and light bands interpreted as manganese oxide tunnels (Turner and Buseck, 1981). A characteristic feature of these sheets is the presence of twinning at 120° (trillings). The basic tunnel width of todorokite is three [$Mn^{4+}O_6$] octahedral chains, or about 9.6 Å (Siegel and Turner, 1982), but natural todorokites contain a variety of tunnel dimensions (Turner *et al.*, 1982). At the present time the term todorokite is widely accepted for the complex tunnel structure in both marine and terrestrial deposits which give an X-ray diffraction pattern with major lines at, or close to, 9.6, 4.8, 2.4, and 1.4 Å (Burns and Burns, 1977). Whether this tunnel structure is the *only* phase in marine nodules giving an X-ray pattern similar to the above is still under investigation (Chukhrov *et al.*, 1983).

This paper is not directed at the question of todorokite crystal structure but at its chemical composition. This is known to be complex and variable (Burns and Burns, 1977). A number of approximate formulae exist. That of Frondel *et al.* (1960), $(Ca,Na,K,Ba,Ag)(Mg,Mn^{2+},Zn)Mn_3^{4+}O_{12} \cdot xH_2O$ is widely used. The most recent paper on todorokite (Burns *et al.*, 1983) indicates that the large cations Ca^{2+}, Ba^{2+}, Na^+, and K^+ occupy the tunnels between the [$Mn^{4+}O_6$] chains while ions such as Mg^{2+} and Zn^{2+} substitute for Mn^{2+} in the

Table I. Electron probe Microanalyses of todorokite (wt.%)

	MnO$_2$	CaO	BaO	MgO	Na$_2$O	K$_2$O	Fe$_2$O$_3$	Al$_2$O$_3$	SiO$_2$	NiO	CuO	CoO	ZnO	H$_2$O+*
1	82.6	0.1	1.8	1.3	0.3	1.2	0.2	0.3	1.2	ND	0.1	0.3	ND	10.6
2	80.6	0.1	2.2	0.8	0.2	1.7	0.3	1.2	1.4	ND	0.2	ND	ND	11.3
3	80.9	0.2	1.7	2.1	0.4	1.8	0.2	1.1	0.8	ND	ND	ND	ND	10.8
4	78.1	ND	3.4	1.9	0.7	3.2	0.1	0.7	0.6	ND	ND	0.1	ND	11.2
5	79.9	ND	3.2	0.8	1.0	1.7	0.1	1.3	1.7	ND	ND	ND	ND	10.4
6	80.2	ND	1.9	0.7	0.8	1.4	0.1	0.8	2.1	ND	ND	ND	ND	12.1
7	82.4	2.1	0.8	1.2	0.2	0.3	0.1	0.4	0.8	ND	ND	ND	ND	11.8
8	82.1	1.8	1.2	1.3	0.3	0.8	0.3	0.3	0.9	ND	ND	ND	0.1	10.9
9	79.6	3.3	1.4	0.8	0.4	0.9	0.4	0.7	1.3	ND	ND	ND	0.1	11.1
10	79.6	2.7	2.2	1.7	0.1	0.4	0.2	1.1	1.1	ND	ND	ND	ND	10.8
11	81.1	ND	1.4	0.4	0.1	0.4	0.6	1.6	2.0	ND	1.2	ND	0.7	10.5
12	81.5	ND	2.8	0.2	0.8	0.8	0.1	1.0	1.4	ND	ND	ND	0.2	11.2
13	80.2	0.7	1.7	ND	1.1	0.9	0.8	0.8	1.2	ND	ND	0.3	0.8	11.8
14	80.4	1.2	1.6	ND	ND	1.1	1.3	0.7	0.7	ND	ND	ND	0.9	12.1
15	79.4	1.8	0.2	0.2	0.6	1.1	1.7	0.4	0.2	0.1	ND	ND	0.5	10.8
16	80.5	1.1	ND	1.1	1.4	1.6	0.2	1.4	0.2	0.7	0.02	ND	0.3	11.3
17	80.9	1.8	ND	0.7	0.8	1.8	ND	1.8	0.8	ND	ND	ND	0.3	11.1
18	80.3	2.2	1.2	0.4	0.6	1.7	ND	0.1	1.2	ND	ND	ND	0.2	12.1
19	81.9	1.7	0.4	ND	1.7	ND	ND	0.1	3.3	ND	ND	ND	ND	10.9
20	75.0	1.4	0.8	ND	ND	1.6	0.1	ND	0.6	0.1	ND	ND	ND	10.4
21	82.2	2.3	1.7	1.8	0.1	0.2	0.8	ND	0.1	0.2	ND	0.8	ND	9.8
22	79.7	2.1	1.4	1.4	0.1	0.6	1.7	0.8	0.1	0.7	ND	1.1	ND	10.3
23	79.3	0.9	2.3	2.2	0.8	ND	ND	1.2	0.8	ND	1.1	0.7	ND	10.7
24	77.4	1.4	1.9	1.7	0.1	1.4	ND	1.7	2.2	ND	ND	0.2	0.8	11.2
25	79.6	1.7	4.2	1.4	0.3	1.2	ND	ND	1.4	ND	ND	0.4	ND	9.8
26	84.2	1.8	1.6	0.2	0.4	1.0	ND	ND	ND	ND	0.4	ND	ND	10.4
27	80.2	2.2	1.8	0.8	0.6	1.6	0.8	ND	ND	ND	0.8	0.2	0.2	10.8
28	78.6	1.9	2.2	0.7	0.5	1.7	0.7	0.6	ND	ND	1.2	0.7	ND	11.2
29	77.9	1.2	0.2	0.3	1.1	1.6	0.7	1.2	1.1	1.7	1.9	0.4	ND	10.7
30	75.9	1.9	0.8	0.4	1.8	1.4	0.4	1.4	0.6	2.4	2.2	0.6	ND	10.2
31	77.7	2.2	0.1	0.8	1.3	0.5	1.6	1.8	0.7	0.2	1.5	1.7	ND	9.9
32	76.4	1.8	0.1	1.2	1.4	0.7	1.4	0.4	1.2	2.8	1.4	0.8	ND	10.4
33	79.3	3.4	ND	0.1	0.8	0.8	2.1	0.5	0.6	0.7	0.3	0.2	ND	11.2
34	78.9	1.7	ND	0.1	1.3	1.4	1.6	0.7	1.6	0.9	0.8	0.2	ND	10.8
35	74.2	1.3	ND	0.7	1.6	1.7	3.8	ND	1.4	1.6	1.2	0.6	ND	10.9

Analyses 1-6 Groote Eylandt "G" quarry; 7-10, in Groote Eylandt Country Rock; 11-15, Gladstone area, Queensland; 16-20 Pilbara, Western Australia; 21-28, Kalgoorlie area, Western Australia; 29-32, Pacific Ocean; 33-35, East Indian Ocean.
ND not detected   Fe$_2$O$_3$, Al$_2$O$_3$ and SiO$_2$ are components of associated silicates and iron oxides
* by difference

tunnel 'walls'. These authors claim that the elements Ni and Cu, which make the manganese nodules potential ore sources, are also able to substitute for Mn^{2+} in the walls.

The range of elements essential to todorokite is as yet unresolved. One difficulty with todorokite (and other manganese oxides) is that it commonly alters to a range of minerals including pyrolusite (Ostwald, 1982a), cryptomelane (Chukhrov et al., 1978), vernadite (Chukhrov et al., 1980), and possibly birnessite (Chukhrov et al., 1978), each mineral having its own suite of component elements. Thus both bulk analyses and electron probe microanalyses (EPMA) may be in error because of heterogeneity. The aim of this research has been to produce chemical analyses, by EPMA, on todorokite samples of optimum homogeneity, and thus to gain some ideas of the range of elements found in both terrestrial and marine specimens of this mineral.

Evaluation of todorokite homogeneity. All the terrestrial samples examined in this study were from Australian deposits, most being collected by the writer. Locations are listed in Table I. The marine todorokites come from the Pacific Ocean

(Ostwald, 1982b) and the SE Indian Ocean (Ostwald, 1984a).

The primary identification of todorokite in the manganese oxide specimens was based on optical microscopy of polished mineragraphic specimens. Well-crystallized todorokite (rare in the samples studied) commonly has a finely acicular form, moderate reflectivity R(589 mn) 10-17%, and definite anisotropism. Most examples are finely polycrystalline, but the reflectivity range is generally sufficient to distinguish this mineral from the low reflectivity, isotropic vernadite (fig. 1), and the higher reflectivity minerals romanechite, cryptomelane, pyrolusite and birnessite.

Confirmation of todorokite occurrence requires X-ray diffraction (XRD) and transmission electron microscopy (TEM). Infra-red (IR) spectroscopy may give additional confirmation. These techniques will also indicate the possible presence of other manganese oxide minerals.

The XRD pattern of todorokite typically consists of moderately broad lines at 9.6 (100), 4.8 (60), 2.4 (50), and 1.4 Å (50). Variation in the position of these lines, their intensities, and presence of additional lines are described by Burns and Burns

FIG. 1. Optical micrograph of polished section of Groote Eylandt manganese ore showing co-existing todorokite (white) and vernadite (grey). × 280.

(1977). A line near 7 Å is often observed in todorokite specimens. The significance in this line is discussed by Ostwald (1984b). In relation to todorokite homogeneity, the association of a line at 7.1–7.2 Å with a line at 3.6 Å is suggestive of birnessite in the todorokite. A line at 3.14 Å usually indicates transformation of todorokite to pyrolusite.

Powder scrapings from polished sections which gave todorokite lines only were analysed in dispersion by conventional transmission electron microscopy (TEM) and some by high resolution transmission electron microscopy (HRTEM). The presence of acicular or fibrous crystals (fig. 2) showing twinning at 120° (trilling) under low power EM, and abundant parallel dark and light bands
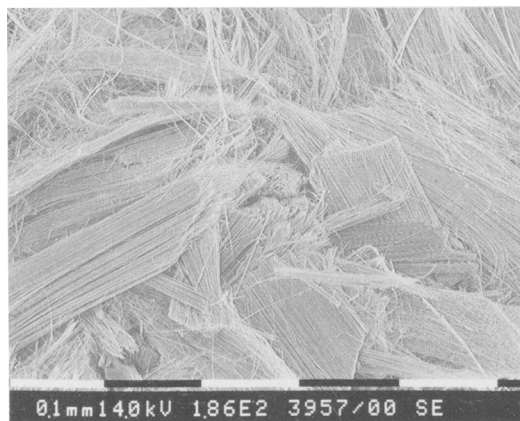

FIG. 2. Scanning electron micrograph of polished surface of todorokite showing the fibrous structure.

commonly at 10 Å separation (tunnel structure) by HRTEM is further confirmation of todorokite.

EM will also show if vernadization of todorokite (Chukhrov et al., 1980) has occurred. This is indicated by the presence of very fine-grained curved platelets (fibrils) developed at the margins of the acicular todorokite crystallites which give select area electron diffraction (SAED) patterns composed of diffraction rings at 2.4, 1.4, sometimes 2.2 Å. The existence of vernadite intergrown with todorokite is not so obvious at higher magnification by HRTEM.

Chemical composition of todorokite—discussion. Fully-ZAF-corrected EPMA analyses on thirty-five areas of todorokite, from eight locations, which have met the criteria of manganese oxide homogeneity just discussed, are listed in Table I. The analyses reveal a number of features of interest in relation to todorokite's chemical composition.

(1) The absence of Ca from the terrestrial todorokite analyses 1–6 and 11, 12 indicates that this element is not as essential to the structure as suggested by Burns and Burns (1978). It would appear, however, that in regions where Ca is absent or in low concentration, Ba may take its place. In the Groote Eylandt manganese ore body, G quarry, the ore contains CaO 0.03%, BaO 1.7%, K_2O 0.5%, and MgO 0.4%, and here a Ba-containing todorokite occurs (Ostwald, 1982a). In the Cretaceous-age sediments which enclose the stratiform manganese oxide deposit, disseminated carbonate ooliths occur in association with a Ca-containing todorokite (Ostwald, 1982b). Most marine nodule todorokites contain Ca, but an analysis reported by Stevenson and Stevenson (1970) apparently contains no CaO, BaO, Na_2O, or MgO.

(2) Analyses 22, 31, suggest that Co occurs in the todorokite structure. The mode of occurrence of Co in marine manganese nodules is a topic which is not fully understood. Statistical analyses of chemical data on whole nodules commonly show correlation between Co and Fe (Burns and Fuerstenau, 1966; Sano and Matsubara, 1970) but sometimes a correlation between Co and Mn (Cronan and Tooms, 1968; Ostwald and Frazer, 1973). The former is usually interpreted as indicating some type of replacement in the ferruginous vernadite (δ-MnO_2) of nodules, possibly as Co^{3+} in the iron-containing component (Burns, 1976). The mode of occurrence of Co in manganese phases in nodules has been discussed by Burns (1976). He concluded that Co^{2+} could be absorbed into a variety of tetravalent manganese oxides, and as low-spin Co^{3+} replace Mn^{4+}. In marine nodules Co which replaces Mn is normally considered to occur in vernadite and Burns (1976) gives as a formula $(Mn,Co^{3+})Mn_6O_{13} \cdot xH_2O$ for this material.

In contrast, Co is not normally included in the various formulae proposed for todorokite (Burns *et al.*, 1983). The analyses in Table I do, however, appear to confirm the ideas of Burns *et al.* (1983) that it is theoretically possible for Co to occur in the todorokite structure.

(3) The concentration of Cu and Ni in todorokite appears to be strongly influenced by the mode of occurrence, with these elements being low to absent from terrestrial todorokite. Terrestrial todorokite in Carinthia (Austria), Cuba, and Portugal (Frondel *et al.*, 1960), Japan (Yoshimura, 1934), and Groote Eylandt (Ostwald, 1982*a, b*) all contain only traces of Ni and Cu. On the other hand there is evidence that the Cu and Ni of the marine manganese nodules is concentrated in the todorokite of these nodules (Burns and Burns, 1977; Cronan, 1980). This pattern of transition element occurrence raises the question as to whether a structural factor is operative. Certainly there is some evidence that different varieties of todorokite exist with ap-parently different capacities for transition elements (Siegel and Turner, 1982; Ostwald, 1982*a, b*) but there is little evidence that this is related to tunnel dimension, etc.

Another explanation, considered more likely by the writer, is that any Ni trapped by manganese oxides in the terrestrial weathering zone will con-centrate in the layer structure minerals lithiophor-ite and asbolane (Chukhrov *et al.*, 1983; Ostwald, 1984*a, b*), minerals which appear to require man-ganese oxide reaction with lateritic gibbsite $Al(OH)_3$ for their formation (Ostwald, 1980). In the writer's opinion lithiophorite is much more com-mon than todorokite in the Australian superficial terrestrial deposits he has studied. On a rare occasion where the two minerals were found in contact, a set of EPMA line scans (MnO_2, Al_2O_3, Cu, Ni, Zn, Co) were made across the contact (fig. 3). It will be seen that the elements Ni, Zn, Cu, and Co all occur preferentially in the lithiophorite.

Lithiophorite does not occur in marine man-ganese nodules, and thus any Cu and Ni trapped by marine manganese oxide gels (Stumm and Giovanoli, 1976) will concentrate in todorokite.

FIG. 3. EPMA line scans across the contact of todorokite and lithiophorite from the Gladstone area, Queensland, Australia.

REFERENCES

Burns, R. G. (1976) *Geochim. Cosmochim. Acta,* **40,** 95–102.
——and Burns, V. M. (1977) In *Marine Manganese Deposits* (G. L. Glasby, ed.), 185–248.
————(1978) *Scanning Electron Microscopy,* SEM Inc., Vol. I, 245–51.
————(1979) *Reviews in Mineralogy,* **6,** 1–40.
——and Fuerstenau, D. W. (1966) *Am. Mineral.* **51,** 895–902.
——Burns, V. M., and Stockman, H. W. (1983) Ibid. **68,** 972–80.
————(1985) Ibid. **70,** 205–8.
Buser, W. (1959) *The nature of the iron and manganese compounds in manganese nodules.* Int. Ocean. Cong. Preprint, **1,** 292–3.
——and Grutter, A. (1956) *Schweiz. Mineral. Petrogr. Mitt.* **36,** 49–62.
Chukhrov, F. V., Gorshkov, A. I., Rudnitskaya, Y. S., Beresovskaya, V. V., and Sivtsov, A. V. (1978) *Int. Geol. Rev.* **22,** 58–74.
————(1980) *Clays Clay Minerals,* **28,** 346–54.
————Beresovskaya, V. V., and Sivtsov, A. V. (1983) *Izv. Akad. Nauk SSSR, Ser. Geol.* **5,** 91–9.
Cronan, D. S. (1980) *Underwater Minerals,* Academic Press, 358 pp.
——and Tooms, J. S. (1968) *Deep-Sea Research,* **16,** 335–59.
Frondel, C., Marvin, U. B., and Ito, J. (1960) *Am. Mineral.* **45,** 1167–73.
Giovanoli, R. (1980) In *Geology and Geochemistry of Manganese,* Vol. 1 (I. M. Varentsov and G. Grasselly, eds.), 159–202.
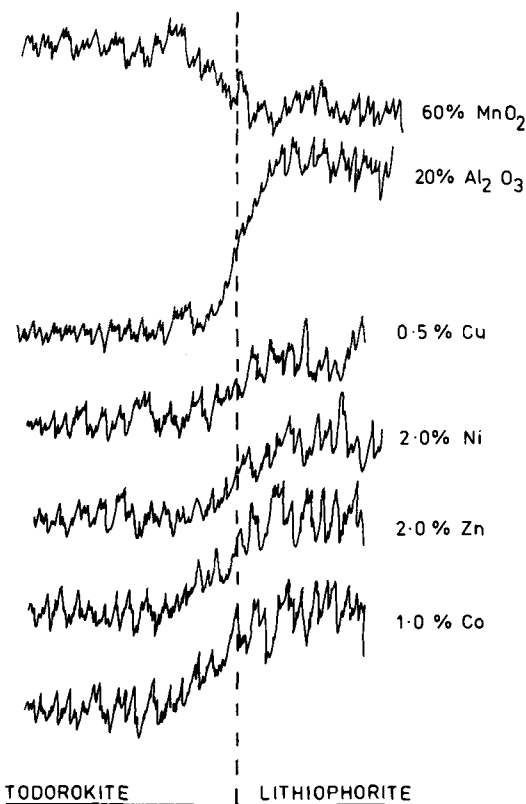——(1985) *Am. Mineral.* **70,** 202–4.

Lallier-Verges, E., and Clinard, C. (1983) *Marine Geol.* **52**, 267–83.

Ostwald, J. (1980) In *Geology and Geochemistry of Manganese*, Vol. 2 (I. M. Varentsov and G. Grasselly, eds.), 149–82.

——(1982*a*) *BHP Tech. Bull.* **26**, 52–6.

——(1982*b*) *Mineral. Mag.* **46**, 253–6.

——(1984*a*) *Geol. Mag.* **121**, 483–8.

——(1984*b*) *Neues Jahrb. Mineral. Mh.* 1–8.

——and Frazer, F. W. (1973) *Mineral. Deposita*, **8**, 303–11.

Sano, M., and Matsubara, H. (1970) *Suiyokwai-Shi*, **17**, 111–14.

Siegel, M. D., and Turner, S. (1982) *Science*, **219**, 172–4.

Stevenson, J. S., and Stevenson, L. S. (1970) *Can. Mineral.* **10**, 599–615.

Stumm, W., and Giovanoli, R. (1976) *Chimia*, **30**, 423–5.

Turner, S., and Buseck, P. R. (1981) *Science*, **212**, 1024–6.

——Siegel, M. D., and Buseck, P. R. (1982) *Nature*, **296**, 841–2.

Wadsley, A. D. (1950) *Am. Mineral.* **35**, 485–99.

Yoshimura, T. (1934) *J. Fac. Sci., Hokkaido Univ.* **4**, 289–97.

The Broken Hill Proprietary Co. Ltd., Central Research Laboratories,   J. OSTWALD
PO Box 188, Wallsend, NSW 2287, Australia

Discussion and comments on the paper: electron-optical studies of phyllosilicate intergrowths in sedimentary and metamorphic rocks

IN a recent paper White *et al.* (1985) discussed the origin and chemistry of phyllosilicate intergrowths in sandstones, shales, metagreywackes, and low-grade schists. They came to an important conclusion, that the origin of chlorite–illite (phengite) intergrowths is mainly by diagenetic and low-grade metamorphic alteration of detrital biotite grains. This conclusion is in good agreement with the observations of the senior author (Morad, 1986) on chlorite–mica (phengite and biotite) intergrowths in shales and sandstones from the Brøttum Formation (Upper Proterozoic; the Sparagmite region of southern Norway). The importance of this agreement in interpretation is that it gives a new view on the origin of such phyllosilicate intergrowths, a matter which is still controversial. Previously, several origins were proposed (see review by Craig *et al.*, 1982), but none could clearly account for, as biotite readily does, the source of ions and the unique pattern of intergrowth.

As experienced by White *et al.* (1985), there are difficulties in obtaining pure chlorite or mica analyses from the intergrowths by means of electron microprobe. Instead, the chlorite analyses often contain K and Ti, while illites show high Fe and Mg contents, and the biotites are greatly depleted in K and/or Fe and Mg. Some analyses of both types of biotite from the Brøttum Formation are given in Table I. A plot of the analyses on an $Al_{total}–(K+Na)$ binary diagram (fig. 1) reveals that those biotites which are mainly depleted in K are characterized by a gradual decrease in interlayer cations and simultaneous increase in total Al, and their general trend is toward chlorite, thus called chloritized biotites here. Most of the analyses of White *et al.* (1985) fall along this trend too (Table II). The second group of biotite analyses (Table I) show higher interlayer cation content, but also a gradual increase in total Al and their trend is toward illite, thus called illitized biotites here. Such biotite compositions, however, were not reported in the paper of White *et al.* (1985) because their analyses were restricted to a biotite grain altered into mainly chlorite, though analysis no. 1 (Table IV of White *et al.*; Table II this paper) is close to illite. The total octahedral occupancies (TOO) of these altered biotites deviate significantly from 6.00 of ideal biotite. The chloritized biotites have TOO greater than 6.00, whereas the illitized biotites have TOO much lower than 6.00, hence confirming the alteration trends above.

The statement made by White *et al.* (1985; p. 420)